AGU PUBLICATIONS

JGR

Journal of Geophysical Research: Space Physics

RESEARCH ARTICLE

10.1002/2014JA020683

Key Points:
- The ion emission route is credible for beam experiments in the magnetosphere
- The electron collection route is not viable
- The background plasma facilitates beam emission

Correspondence to:
G. L. Delzanno,
delzanno@lanl.gov

Citation:
Delzanno, G. L., J. E. Borovsky, M. F. Thomsen, and J. D. Moulton (2015), Future beam experiments in the magnetosphere with plasma contactors: The electron collection and ion emission routes, *J. Geophys. Res. Space Physics*, *120*, 3588–3602, doi:10.1002/2014JA020683.

Received 1 OCT 2014
Accepted 2 MAR 2015
Accepted article online 6 MAR 2015
Published online 19 MAY 2015

Future beam experiments in the magnetosphere with plasma contactors: The electron collection and ion emission routes

G. L. Delzanno[1], J. E. Borovsky[2,3], M. F. Thomsen[4], and J. D. Moulton[1]

[1]Theoretical Division, Los Alamos National Laboratory, Los Alamos, New Mexico, USA, [2]Space Science Institute, Boulder, Colorado, USA, [3]AOSS, University of Michigan, Ann Arbor, Michigan, USA, [4]Intelligence and Space Research Division, Los Alamos National Laboratory, Los Alamos, New Mexico, USA

Abstract Experiments where a high-voltage electron beam emitted by a spacecraft in the low-density magnetosphere is used to probe the magnetospheric configuration could greatly enhance our understanding of the near-Earth environment. Their challenge, however, resides in the fact that the background magnetospheric plasma cannot provide a return current that balances the electron beam current without charging the spacecraft to such high potential that in practice prevents beam emission. In order to overcome this problem, a possible solution is based on the emission of a high-density contactor plasma by the spacecraft prior to and after the beam. We perform particle-in-cell simulations to investigate the conditions under which a high-voltage electron beam can be emitted from a magnetospheric spacecraft, comparing two possible routes that rely on the high-density contactor plasma. The first is an "electron collection" route, where the contactor has lower current than the electron beam and is used with the goal of connecting to the background plasma and collecting magnetospheric electrons over a much larger area than that allowed by the spacecraft alone. The second is an "ion emission" route, where the contactor has higher current than the electron beam. Ion emission is then enabled over the large quasi-spherical area of the contactor cloud, thus overcoming the space charge limits typical of ion beam emission. Our results indicate that the ion emission route offers a pathway for performing beam experiments in the low-density magnetosphere, while the electron collection route is not viable because the contactor fails to draw a large neutralizing current from the background.

1. Introduction

Experiments where a high-power electron beam is emitted by a magnetospheric spacecraft are of interest for studies of magnetosphere-ionosphere connectivity and magnetosphere-ionosphere coupling [*Borovsky et al.*, 2000; *MacDonald et al.*, 2012] and could greatly enhance our understanding of the near-Earth environment.

Electron beam experiments have been successfully operated many times from rockets and spacecraft in the ionosphere, where the ambient plasma is dense [*Hendrickson et al.*, 1975; *Hallinan et al.*, 1978; *Winckler*, 1980; *Pellat and Sagdeev*, 1980; *Zhulin et al.*, 1980; *Swanson et al.*, 1986; *Nemzek and Winckler*, 1991; *Nemzek et al.*, 1992; *Lavergnat*, 1982; *Prech et al.*, 1995, 2002; *Katz et al.*, 1994]. In the ionosphere a sufficient return current can be drawn from the background plasma to balance the electron beam current and to maintain spacecraft charging to low levels that do not prevent beam emission.

Spacecraft charging issues become severe when a high-power electron beam experiment on a spacecraft in the tenuous plasma of the magnetosphere is considered [*Delzanno et al.*, 2015], since in the magnetosphere the thermal fluxes of electrons are orders of magnitude smaller than the electron beam currents of interest. When the electron beam is fired, a residual positive charge will be left on the spacecraft. The problem becomes moving the residual positive charge off of the spacecraft and away from the spacecraft so that voltages associated with that positive charge remain small. Indeed, the spacecraft charging problem for electron beam experiments in the magnetosphere has been pointed out as an outstanding technical issue for space physics [*National Research Council*, 2012].

A possible solution to the spacecraft charging problem involves the operation of a plasma contactor on the magnetospheric spacecraft to emit a dense plasma cloud prior to and during the operation of the electron beam. Plasma contactors are often used to control spacecraft charging [e.g., *Olsen*, 1985; *Schmidt et al,*, 1995; *Comfort et al.*, 1998; *Torkar*, 2001]. They use a noble gas (typically xenon) and less of a kilogram per year of fuel is normally sufficient since they only operate for a few seconds per hour. One can imagine that the contactor plasma reduces the positive charge on the spacecraft by either (a) collecting ambient magnetospheric electrons or (b) emitting ions. In a prior analysis performed in vacuum [*Delzanno et al.*, 2015] it was shown that ion emission from the surface of the contactor plasma cloud into three dimensions may provide a mechanism to allow beam experiments in the magnetosphere to operate.

In this paper, particle-in-cell (PIC) simulations are presented to investigate the viability of the two strategies (electron collection and ion emission) in the presence of the background plasma. Our conclusion is that the electron collection route is not viable. In the case where the contactor is fired only prior to the electron beam, as the spacecraft charges positively because of beam emission and reabsorbs the contactor electrons, the contactor ions are pushed away from the spacecraft and the contact between the two and the ability to draw a large neutralizing current from the background within benign level of spacecraft charging are lost. When the contactor is kept on during beam emission (with the contactor current lower than the beam current), contact between the spacecraft and the ion contactor cloud is maintained, but the contactor still fails to draw a large background current. The ion emission route (in the limit of the contactor current larger than the beam current), on the other hand, does not depend on establishing contact between the spacecraft and the background plasma since it relies only on the ability of the ion contactor cloud to expand to a size where there are no space charge limits on ion emission. Nevertheless, the presence of the background plasma reduces the transient of the spacecraft potential (relative to the limiting case with no background plasma) and helps beam emission. We conclude that the ion emission route offers a strategy for high-voltage high-power beam emission in a low-density magnetosphere.

The paper is organized as follows. In section 2 we discuss the electron collection and ion emission strategies for beam emission in the magnetosphere based on the contactor plasma. In section 3 we present the simulation model and setup. In section 4 we compare simulations of the electron collection and ion emission routes varying parametrically the background plasma density. In section 5 we draw the conclusions of this research.

2. Discussion of Different Strategies for Electron Beam Emission in Space: The Electron Collection and Ion Emission Routes

2.1. The Spacecraft Charging Equation

In order to understand different strategies that could be used for electron beam emission in space, the spacecraft charging equation [*Hastings and Garrett*, 2004]

$$\frac{dQ_{sp}}{dt} = I_b^e + I_e^{bg} + I_i^{bg} + I_e^{cont} + I_i^{cont} \tag{1}$$

is a useful starting point. In equation (1), Q_{sp} is the net charge on the spacecraft, I_b^e is the (constant) electron beam current, I_e^{bg} and I_i^{bg} are the currents associated with the fluxes of magnetospheric (background) electrons and ions to the spacecraft, and I_e^{cont} and I_i^{cont} are the currents associated with the emission of electrons and ions off the spacecraft by the plasma contactor. In equation (1) photoelectron currents and secondary electron currents are ignored. Let us begin by establishing some useful facts. In absence of background plasma and contactor currents and using the charge versus potential relation for a spherical body in vacuum,

$$Q_{sp} = C_{sp}\phi_{sp} = 4\pi\varepsilon_0 r_{sp}\phi_{sp} \tag{2}$$

(ε_0 is the permittivity of vacuum, the spacecraft is spherical with radius r_{sp} and C_{sp} is its capacitance), equation (1) shows that the spacecraft potential ϕ_{sp} grows linearly in time. When the spacecraft potential reaches a value corresponding to the kinetic energy of a beam electron ($e = 1.6 \cdot 10^{-19}$ C is the elementary charge, m_e is the electron mass, and V_b is the velocity of the beam electron)

$$e\phi_{sp}^{ret} = \frac{m_e}{2}V_b^2, \tag{3}$$

the beam returns to the spacecraft. This happens at time

$$t_r = \frac{2\pi\varepsilon_0 r_{sp} m_e V_b^2}{e I_b^e}. \quad (4)$$

For $r_{sp} = 1$ m, $I_b^e = 0.1$ A, and a 1 keV beam, it follows that $\phi_{sp}^{ret} = 1$ kV and $t_r \simeq 1.1$ μs. The beam would only travel 21 m before being electrostatically pulled back.

Let us now consider a system with the beam and the background plasma ($I_{e,i}^{cont} = 0$). The background currents can be estimated using the orbital motion limited (OML) theory [*Mott-Smith and Langmuir*, 1926; *Whipple*, 1981]

$$I_e^{bg} = -e\sqrt{8\pi} r_{sp}^2 n_e \sqrt{\frac{T_e}{m_e}} \left(1 + \frac{e\phi_{sp}}{T_e}\right), \quad (5)$$

$$I_i^{bg} = e\sqrt{8\pi} r_{sp}^2 n_i \sqrt{\frac{T_i}{m_i}} \exp\left(-\frac{e\phi_{sp}}{T_i}\right), \quad (6)$$

valid when $\phi_{sp} > 0$. In equations (5) and (6), m_i is the ion mass while $n_{e(i)}$ and $T_{e(i)}$ are the magnetospheric background electron (ion) density and temperature (expressed in eV). Note that the OML theory assumes spherical symmetry, neglects potential barriers to the particle motion, and neglects magnetic field effects [*Mott-Smith and Langmuir*, 1926; *Al'pert et al.*, 1965; *Laframboise*, 1966; *Allen et al.*, 2000; *Tang and Delzanno*, 2014]. It is normally applicable in the small spacecraft/probe radius relative to the plasma Debye length and the plasma gyroradii, although simulations have shown that OML can still be an excellent approximation even for probe radii of the order of the Debye length or the electron gyroradius [*Delzanno et al.*, 2004, 2013]. The theory could also be generalized to nonsymmetric potentials following the approach discussed by *Laframboise and Parker* [1973]. The equilibrium of equation (1) with currents given by equations (5) and (6) can be calculated numerically to understand what level of the spacecraft potential is necessary to draw a current from the magnetospheric plasma that can balance I_e^b. For approximate plasma parameters at the geosynchronous orbit ($n_e = n_i = 1$ cm^{-3}, $T_e = T_i = 1$ keV, $m_i/m_e = 1836$, $B = 100$ nT, Debye length ~ 235 m, and electron gyroradius ~ 750 m) the conditions for the validity of OML are met for a spacecraft with $r_{sp} = 1$ m. For $I_b^e = 0.1$ A, the equilibrium of the spacecraft potential is reached at $\phi_{sp}^{eq} = 9.4 \cdot 10^6$ V, i.e., the spacecraft would need to be at a potential of +9.4 MV to draw in enough magnetospheric electrons to balance the current of the electron beam. For a 1 keV beam, $\phi_{sp}^{eq} = 9.4 \cdot 10^6$ V is orders of magnitude higher than $\phi_{sp}^{ret} = 1$ kV, implying that the beam returns to the spacecraft as it would do without any background plasma. It is clear that the return current provided by the background plasma is insufficient to allow emission of a high-voltage electron beam in the low-density magnetosphere and some other strategy must be conceived. Inspection of equation (5) reveals ways that can increase the electron magnetospheric current: in order of importance given by the exponent of the power law, larger collection areas (r_{sp}^2), larger background density (n_e), and larger temperature ($\sqrt{T_e}$) lead to larger electron currents from the background. Figure 1 shows ϕ_{sp}^{eq} varying with n_e (left) and r_{sp} (right). The dashed line shows $\phi_{sp}^{ret} = 1$ kV and represents the limit above which a 1 keV electron beam cannot be emitted by the spacecraft. Figure 1 shows that background densities $n_e > 5 \cdot 10^3$ cm^{-3} or collection radii > 70 m allow beam emission. Both of these options are impractical.

2.2. Different Routes to Allow Electron Beam Emission in Space

A strategy presented in *Borovsky et al.* [2000] and *MacDonald et al.* [2012] to overcome the problems discussed in the previous subsection relies on emitting a high-density neutral contactor plasma prior to and during beam emission. We begin by considering the case where the contactor current is lower than the beam current. The contactor plasma creates a high-density plasma reservoir near the spacecraft that provides a large (relative to the background current) electron current that can compensate for that of the electron beam. Over time this leaves behind a positively charged contactor cloud. Let us first estimate what size of the contactor cloud would be necessary to allow beam emission. Assuming that the electron beam emitted charge Q is transferred to the area enclosed by the spacecraft and the ion contactor cloud (which is at potential ϕ and is described by a spherical characteristic radius R), from equation (2) one has

$$R = \frac{Q}{4\pi\varepsilon_0\phi}. \quad (7)$$

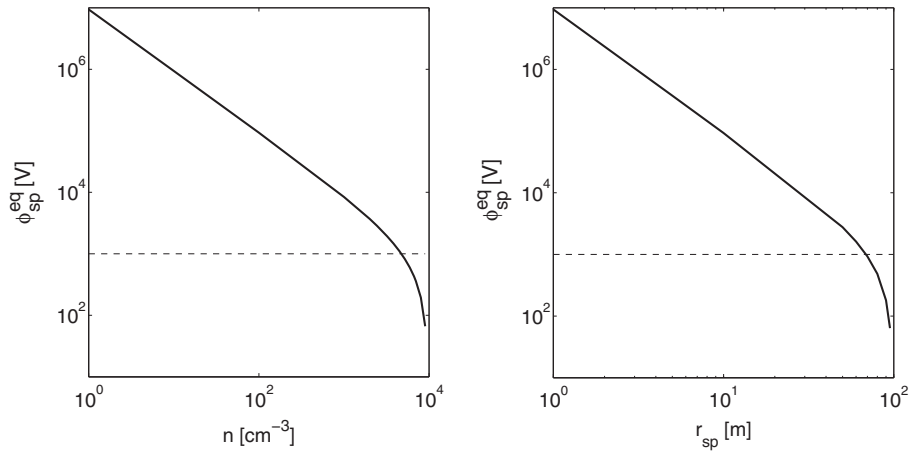

Figure 1. The equilibrium spacecraft potential obtained from equation (1) with $I_b^e = 0.1$ A and $I_{e,i}^{bg}$ given by equations (5) and (6), varying (left) the background plasma density $n_e = n_i$ ($r_{sp} = 1$ m) and (right) the collection radius r_{sp} ($n_e = n_i = 1$ cm^{-3}). The dashed line is ϕ_{sp}^{ret} given by equation (3). Other parameters are $m_i/m_e = 1836$, $T_e = T_i = 1$ keV, and $V_b = 1.9 \cdot 10^7$ m/s.

For a 1 keV electron beam with $I_b^e = 0.1$ A that released $Q = 0.25$ C and keeping $\phi < \phi_{sp}^{ret}$ to allow beam emission, it follows that the contactor cloud characteristic radius would be $R \gtrsim 2.2 \cdot 10^3$ km, i.e., of the order of the size of the Earth. Note that this is much larger than what was found in Figure 1 (right) since there the equilibrium charge corresponding to $\phi_{sp}^{eq} = 9.4$ MV is $Q_{sp} = 10^{-3}$ C, much smaller than the $Q = 0.25$ C considered here, because of the contribution of the background currents. Since creating a contactor cloud as big as the Earth is clearly impractical, one can imagine employing a smaller contactor cloud whose purpose is to make contact with the background magnetospheric plasma: as the beam is emitted and the contactor cloud charges positively, a neutralizing electron current from the background magnetospheric plasma is drawn to reduce the net charge in the cloud (c.f. equation (1)). From Figure 1 one suspects that a kilometer-sized cloud should be sufficient to compensate for the electron beam current (although magnetic field effects not accounted for in Figure 1 will affect current collection for a large contactor cloud [*Parker and Murphy*, 1967; *Laframboise and Sonmor*, 1993]). We will refer to this strategy as the *electron collection route*, since the electron beam current is ultimately balanced by an electron magnetospheric current collected over a larger area. An obvious challenge of this approach is that, in the absence of collisions, background electrons could be accelerated through the contactor cloud but without being trapped in it and might therefore fail to deliver the necessary current to the spacecraft.

Of course, one can think of a strategy that uses an ion current emitted by the spacecraft to balance the electron beam current. We note that a naive view of equation (1) would suggest that one could balance I_b^e by emitting an ion beam I_b^i of equal current, $I_b^i = I_b^e$, without the need for a contactor plasma. In practice, however, this idea does not work because for parameters of interest the ion beam current is above the Child-Langmuir space charge limit [*Child*, 1911] and only a small fraction of the ion beam current can really be emitted [*Wang and Lai*, 1997; *Delzanno et al.*, 2015]. On the other hand, a different strategy to enable electron beam emission in space, again based on the plasma contactor, was put forward in *Delzanno et al.* [2015]. It consists of operating the electron beam and the contactor simultaneously but with $I_b^e < I_i^{cont}$. In this case, the role of the contactor is to enable ion emission over a large, quasi-spherical area (unlike the case of the ion beam which occurs on a small, planar area which is strongly space charge limited). Thus, the transient of the spacecraft potential is kept under control because the spacecraft is able to emit an ion current larger than the beam current. We will refer to this strategy as the *ion emission route*.

In section 4 we will perform particle-in-cell (PIC) simulations to compare and contrast the electron collection and ion emission routes. The validity of the latter has already been established in *Delzanno et al.* [2015] but for electron beam and contactor emitted in vacuum. Here we will complement the results of *Delzanno et al.* [2015] by exploring the role played by the background plasma.

3. Simulation Model and Setup

In this paper we study the interaction of a spherical spacecraft with a plasma made of electrons and singly charged hydrogen ions. The plasma consists of a magnetospheric background population and the contactor plasma emitted by the spacecraft. The spacecraft also emits an electron beam.

The system is modeled by the Curvilinear particle-in-cell (CPIC) code which solves the collisionless Vlasov equation in the electrostatic limit, where the dynamics of the plasma is governed by the self-consistent electric field arising from its charge distribution and by an external, constant magnetic field $\mathbf{B}_0$. The model equations read

$$\frac{\partial f_s}{\partial \tau} + \hat{\mathbf{v}} \cdot \nabla_{\hat{x}} f_s + \frac{q_s}{e}\frac{m_e}{m_s}\left(-\nabla\psi + \hat{\mathbf{v}} \times \hat{\mathbf{B}}_0\right) \cdot \nabla_{\hat{v}} f_s = 0, \tag{8}$$

$$-\nabla^2\psi = \sum_s \frac{q_s}{e}\hat{n}_s, \tag{9}$$

In equation (8), f_s is the plasma distribution function and s labels each plasma species ($s = e$, i, and b for electrons, ions, and the beam, respectively), τ is time, $\hat{\mathbf{x}}$ and $\hat{\mathbf{v}}$ are position and velocity, q_s (m_s) is the charge (mass) for each species, and ψ is the electrostatic potential. Note that we have lumped the background and contactor plasma components together, but later we will use the superscripts "bg" and "cont" to specify their parameters separately.

Equations (8) and (9) are normalized as follows. We introduce a reference density n_{ref} and temperature T_{ref}. Lengths are normalized to a reference Debye length $\lambda_{\text{ref}} = \sqrt{\frac{\epsilon_0 T_{\text{ref}}}{e^2 n_{\text{ref}}}}$, $\hat{\mathbf{x}} = \mathbf{x}/\lambda_{\text{ref}}$; velocity to the reference electron thermal velocity $v_{\text{th,ref}} = \sqrt{\frac{T_{\text{ref}}}{m_e}}$, $\hat{\mathbf{v}} = \mathbf{v}/v_{\text{th,ref}}$; time to the reference electron plasma frequency $\omega_{\text{pe,ref}} = \sqrt{\frac{e^2 n_{\text{ref}}}{\epsilon_0 m_e}}$, $\tau = \omega_{\text{pe,ref}} t$; densities to a reference density, $\hat{n}_s = n_s/n_{\text{ref}}$; temperatures to a reference temperature, $\hat{T}_s = T_s/T_{\text{ref}}$; the electrostatic potential is normalized as $\psi = e\phi/T_{\text{ref}}$; and the background magnetic field as $\hat{\mathbf{B}}_0 = \frac{\omega_{\text{ce,ref}}}{\omega_{\text{pe,ref}}}\frac{\mathbf{B}_0}{|\mathbf{B}_0|}$, with the reference electron cyclotron frequency given by $\omega_{\text{ce,ref}} = e|\mathbf{B}_0|/m_e$.

The model equations are solved numerically with the particle-in-cell (PIC) technique *Birdsall and Langdon* [1985], implemented in a recently developed code called Curvilinear PIC (CPIC) [*Delzanno et al.*, 2013]. CPIC has been used primarily for studies of the interaction between plasmas and material objects [*Delzanno et al.*, 2013; *Delzanno and Tang*; 2014]. We run CPIC in cylindrical (r, θ, z) geometry and impose azimuthal symmetry on the electrostatic field. The particles retain three components of the velocity, namely, we run CPIC in the so-called 2D3V formulation [*Birdsall and Langdon*, 1985]. The simulation domain is enclosed by two concentric spheres of radius ρ_{sp} and ρ_2, where we have introduced $\rho = \sqrt{r^2 + z^2}$, and the spacecraft of radius ρ_{sp} represents the inner boundary of the simulation domain. Particles that hit the spacecraft are removed from the simulation and their charge is accumulated onto the spacecraft. The spacecraft is assumed to be a perfect conductor, and the spacecraft accumulated charge $\hat{Q}_{\text{sp}}$ yields a boundary condition at $\rho = \rho_{\text{sp}}$ given by Gauss's law. Particles can leave the system at the outer boundary, where a Dirichlet (conducting) boundary condition is applied on the electrostatic potential: $\psi\left(\rho_2\right) = 0$. The background magnetic field is directed along z.

The contactor plasma is injected at $\rho = \rho_{\text{sp}}$ antiparallel to $\hat{\mathbf{B}}_0$. At injection, the contactor is characterized by density $\hat{n}_{e,i}^{\text{cont}}$, temperature $\hat{T}_{e,i}^{\text{cont}}$, and ion drift velocity $\hat{V}_i^{\text{cont}}$ directed along $-z$. Electrons are injected in the system according to a Maxwellian distribution at rest since their thermal velocity is much larger than the drift velocity. Ions, on the other hand, are in the opposite limit and their injection velocity is mostly given by the drift velocity plus a small thermal spread. When the contactor injection is on, we introduce 400 macroparticles per species per time step.

The background plasma is present at all times of the simulation. At time $\tau = 0$ it is loaded in the system according to a Maxwellian distribution at rest with density $\hat{n}_{e,i}^{\text{bg}}$ and temperature $\hat{T}_{e,i}^{\text{bg}}$ equal for electrons and ions. At every time step, we inject particles at the outer boundary $\rho = \rho_2$ to compensate for the thermal flux of background particles that leaves the system. This allows one to simulate an infinite background plasma medium outside the simulation domain [*Birdsall and Langdon*, 1985]. At time $\tau = 0$ we load 49 macroparticles per cell, and the number of injected particles per time step is such to keep a similar level of resolution throughout the simulation.

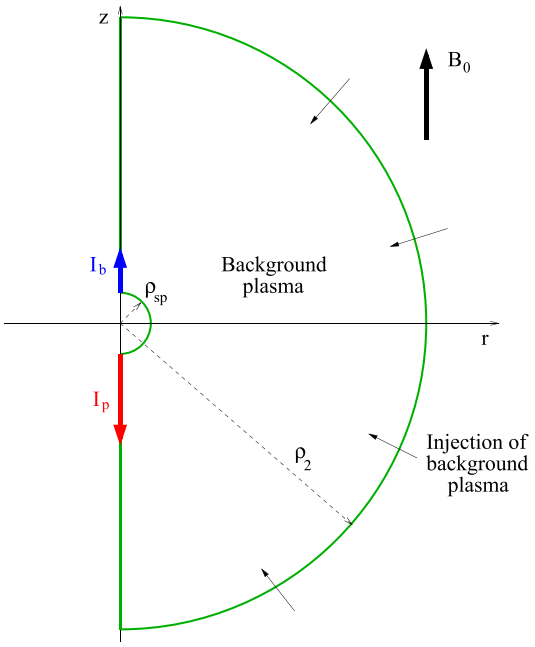

Figure 2. Cartoon of the simulation setup. Since for the parameters considered in this study the background plasma gyroradii are much larger that the spacecraft radius, current collection from the background plasma occurs as if the plasma were unmagnetized.

We simulate the effect of the electron beam by removing the beam charge $\hat{I}_b \Delta\tau$ ($\hat{I}_b$ is the beam current) at every time step $\Delta\tau$. This is equivalent to a beam with infinite kinetic energy and it is a conservative choice in terms of the transient induced on the spacecraft potential (since beam electrons cannot be pulled back electrostatically and return to the spacecraft), as shown in *Delzanno et al.* [2015].

A cartoon of the simulation setup can be found in Figure 2.

The following dimensionless parameters are considered in this study:

1. Background magnetic field magnitude: $\hat{B}_0 = 3 \cdot 10^{-3}$.
2. Geometrical parameters: $\rho_{sp} = 1$, $\rho_2 = 50$.
3. Background plasma parameters: $\frac{m_i}{m_e} = 1836$, $\hat{n}^{bg} = \hat{n}_e^{bg} = \hat{n}_i^{bg}$, $\hat{T}_e^{bg} = \hat{T}_i^{bg} = 1$.
4. Contactor plasma parameters: $\frac{m_i}{m_e} = 1836$, $\hat{n}_e^{cont} = \hat{n}_i^{cont} = 100$, $\hat{V}_i^{cont} = 0.01$, $\hat{T}_e^{cont} = \hat{T}_i^{cont} = 0.01$, $\hat{I}_i^{cont} = 0.187$.

In these units the background plasma Debye length is $\hat{\lambda} = 1/\sqrt{\hat{n}^{bg}}$ and the electron gyroradius is $\hat{\rho}_e = \omega_{pe,ref}/\omega_{ce,ref}$ ($\hat{T}_e^{bg} = 1$). For the parameters of this study ($\hat{n}^{bg} = 10^{-4}$ and $\hat{n}^{bg} = 10^{-2}$), both quantities are much larger than ρ_{sp} and justify the use of OML current collection for the estimates of section 4. The majority of the simulations will be conducted with $\hat{I}_b = 0.093 = \hat{I}_i^{cont}/2$ but we will study a few cases with $\hat{I}_b = 0.374 = 2\hat{I}_i^{cont}$. Except for the presence of the background plasma and the case $\hat{I}_b = 0.374$, these are the same parameters used in *Delzanno et al.* [2015]. As discussed in *Delzanno et al.* [2015], these parameters are somewhat rescaled relative to a realistic system. For reference, one can assume $n_{ref} = 10^4$ cm^{-3}, $T_{ref} = 1$ keV, and $|\mathbf{B}_0| = 100$ nT, which would give a contactor ion current $I_i^{cont} = 0.022$ A.

The simulations are conducted with a 4096×1024 grid in (r, z) and time step $\Delta\tau = 0.02$, using 256 cores of the Mapache cluster at the Los Alamos National Laboratory. Some convergence study was performed with $\Delta\tau = 0.01$ without appreciable changes in the results.

The simulation campaign is conducted as follows. Initially, we perform simulations where we only inject the contactor plasma and follow its expansion in the background plasma. Three configurations obtained at $\tau = 200, 600, 1000$ (labeled as Cases 1, 2, and 3) are then used as initial conditions for studies of beam emission from the spacecraft. We compare simulations of beam emission when the contactor injection is turned off at the time the beam is turned on (i.e., the electron collection route in the limiting case $\hat{I}_b/\hat{I}_i^{cont} \longrightarrow \infty$) to ones where the contactor injection remains on when the beam is turned on (the electron collection route with $\hat{I}_b > \hat{I}_i^{cont}$ and the ion emission route with $\hat{I}_b < \hat{I}_i^{cont}$). We will vary the background density $\hat{n}^{bg}$ parametrically to investigate its role. The ion densities of the three initial configurations of Cases 1, 2, and 3 for $\hat{n}_{bg} = 10^{-4}$ are plotted in Figure 3.

4. Results

Let us begin by analyzing simulations of beam emission with contactor injection turned off when the beam with $\hat{I}_b = 0.093$ is turned on. Figure 4 shows the spacecraft potential ψ_{sp} versus time for the three initial configurations of the contactor plasma that were discussed in section 3 (cf. Figure 3). These simulations are performed for a low-density background $\hat{n}_e^{bg} = \hat{n}_i^{bg} = 10^{-4}$. The dots in Figure 4 mark the time where the total amount of charge emitted by the electron beam is (approximately) equal to the charge that was present in each contactor species at $\tau = 0$. For each curve, the behavior of ψ_{sp} is monotonically increasing

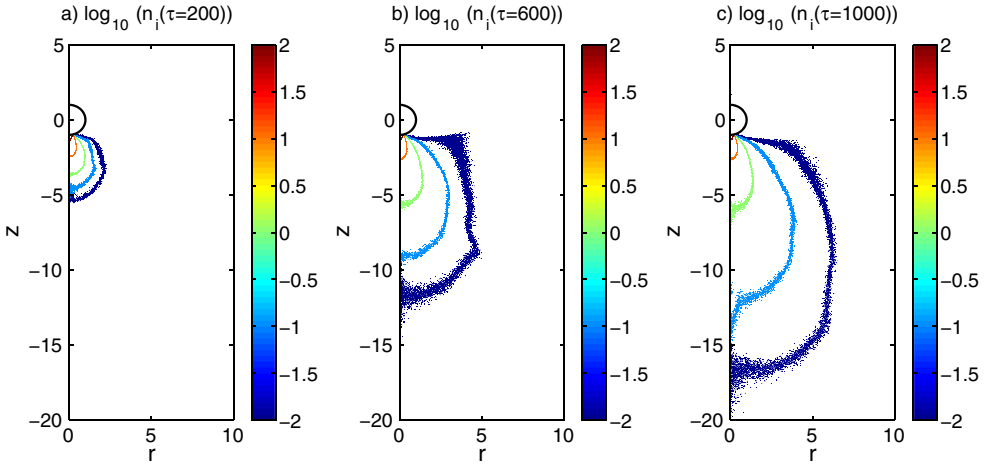

Figure 3. Contours of the three configurations of the ion density at times $\tau = 200$, 600, and 1000 (labeled as Cases 1, 2, and 3) obtained by injecting the contactor in the background plasma without beam emission. These are used as initial conditions for the studies of beam emission from the spacecraft presented in section 4. The background density is $\hat{n}^{bg} = 10^{-4}$ and is not visible in the plots.

with time (except at time τ=0 where there is a short initial transient where the spacecraft potential decreases with time but is not really visible in Figure 4), rising slowly at early times and faster at the end of the simulation. The initial slope of the spacecraft potential can be estimated as done in *Delzanno et al.* [2015] via a capacitance-type argument. Assuming that the electron charge emitted by the beam is transferred to the spacecraft and the ion contactor cloud (characterized by a capacitance $\hat{C}_{cont}$ and assumed at $\psi = \psi_{sp}$), it is easy to obtain

$$\frac{d\psi_{sp}}{d\tau} \simeq \frac{\hat{I}_b}{\hat{C}_{cont}}. \tag{10}$$

In order to obtain the capacitance $\hat{C}_{cont}$, for each contactor plasma configuration at $\tau = 0$ we calculate the area $\mathcal{A}_{i,10^{-3}}$ of the ion density contour corresponding to $\hat{n}_i = 10^{-3}$, calculate the equivalent spherical radius $\mathcal{R}_{i,10^{-3}} = \sqrt{2\mathcal{A}_{i,10^{-3}}/\pi}$, and use it to obtain $\hat{C}_{cont} = 4\pi\mathcal{R}_{i,10^{-3}}$. For the three initial contactor configurations of Figure 3, we find $\mathcal{R}_{i,10^{-3}} = 2.5$, 7.1, and 10.4, leading to $d\psi_{sp}/d\tau \simeq 2.9 \cdot 10^{-3}$, $1.1 \cdot 10^{-4}$, and $7.2 \cdot 10^{-4}$. This is in good agreement with a numerical evaluation of $d\psi_{sp}/d\tau$ by finite difference approximation between $\tau = 20$ and $\tau = 60$: $d\psi_{sp}^{num}/d\tau \simeq 3.2 \cdot 10^{-3}$, $9.8 \cdot 10^{-4}$, and $6.6 \cdot 10^{-4}$.

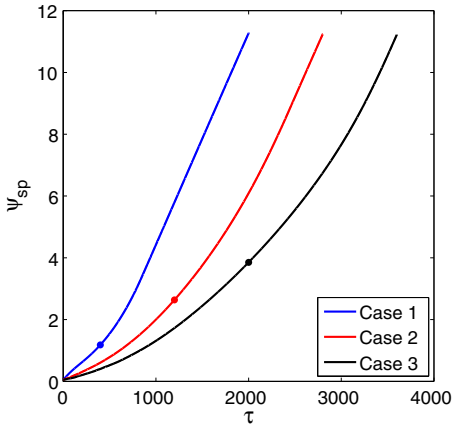

Figure 4. Spacecraft potential versus time starting from the three initial contactor configurations described in section 3, with the injection of the contactor turned off while the beam is emitted. The dots mark the time where the electron beam has injected an amount of charge equal to that present in each contactor species at $\tau = 0$. The background plasma density is $\hat{n}^{bg} = 10^{-4}$ and $\hat{I}_b = 0.093$.

As time progresses the spacecraft potential rises at a faster pace than at the beginning and asymptotically all the curves reach the same growth rate. This asymptotic state can be calculated via equations (1) and (5), which can be solved analytically if we neglect the ion current from the magnetosphere (as justified by the fact that the spacecraft is accumulating a strong positive charge). This leads to the solution

$$\psi_{sp} = \left(1 - \frac{\hat{I}_b}{\sqrt{8\pi}\rho_{sp}^2\hat{n}_e^{bg}}\right)\left[\exp\left(-\frac{\rho_{sp}\hat{n}_e^{bg}\tau}{\sqrt{2\pi}}\right) - 1\right], \tag{11}$$

where we have assumed that $\psi_{sp}(0) = 0$. In the limit $\hat{n}_e^{bg}\tau/\sqrt{2\pi} \ll 1$ (late time in Figure 4) and considering that $\hat{I}_b/\hat{n}_e^{bg} \gg 1$, equation (11) simplifies to

$$\psi_{sp} \simeq \frac{\hat{I}_b}{4\pi\rho_{sp}}\tau \longrightarrow \frac{d\psi_{sp}}{d\tau} \simeq \frac{\hat{I}_b}{\hat{C}_{sp}}, \tag{12}$$

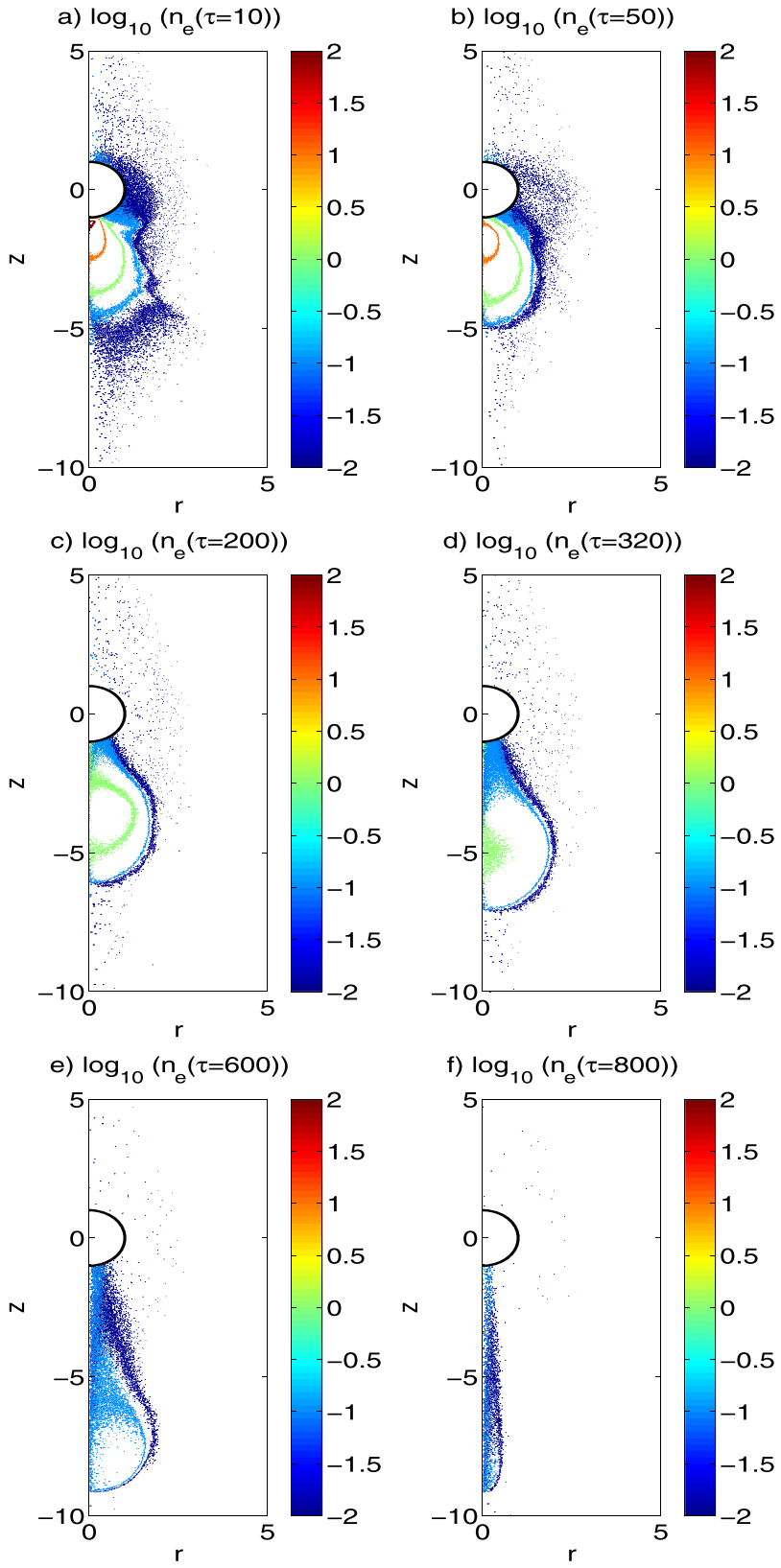

Figure 5. Electron density contours corresponding to $\hat{n}_e = 10^2, 10^1, 10^0, 10^{-1}$, and 10^{-2} at various times for Case 1 with the contactor injection turned off. The background plasma density is $\hat{n}^{bg} = 10^{-4}$ and $\hat{I}_b = 0.093$.

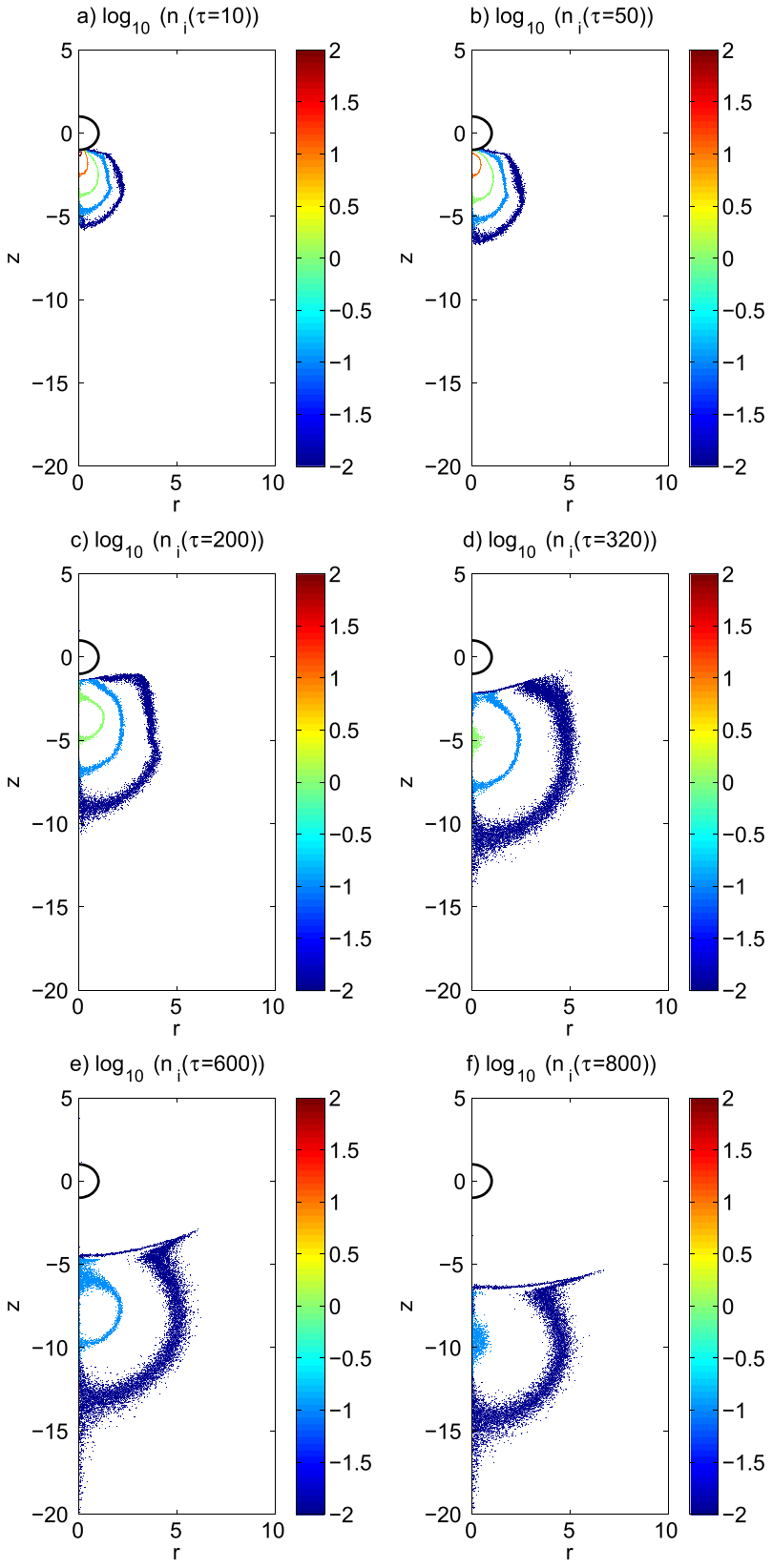

Figure 6. Ion density contours corresponding to $\hat{n}_i = 10^2$, 10^1, 10^0, 10^{-1}, and 10^{-2} at various times for Case 1 with the contactor injection turned off. The background plasma density is $\hat{n}^{bg} = 10^{-4}$ and $\hat{I}_b = 0.093$.

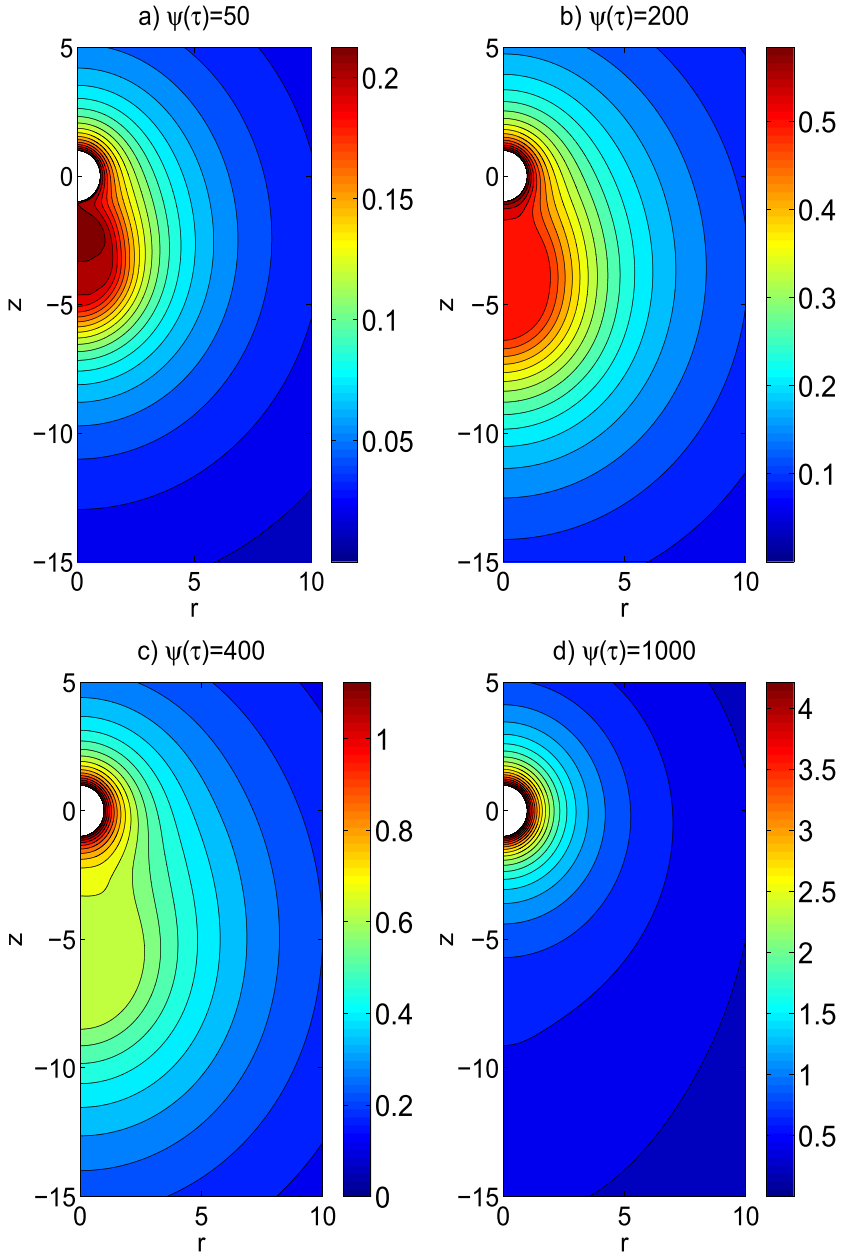

Figure 7. Potential near the spacecraft at various times for Case 1 with the contactor injection turned off. The background plasma density is $\hat{n}^{bg} = 10^{-4}$ and $\hat{I}_b = 0.093$.

indicating that on this time scale the spacecraft potential rises linearly in time driven by electron beam emission and without much contribution from the background electrons. From equation (12), one obtains $d\psi_{sp}/d\tau \simeq 7.4 \cdot 10^{-3}$, in good agreement with the numerical calculation of $d\psi_{sp}/d\tau$ at the end of each simulation which gives $d\psi_{sp}^{num}/d\tau \simeq 6.8 \cdot 10^{-3}$ for all curves. For $\hat{n}_e^{bg}\tau/\sqrt{2\pi} \gg 1$, the spacecraft potential reaches its equilibrium value where the electron beam and background currents balance. For $\hat{n}^{bg} = 10^{-4}$, equation (11) yields

$$\psi_{sp}^{eq} = \frac{\hat{I}_b}{\sqrt{8\pi}\rho_{sp}^2 \hat{n}_e^{bg}} - 1 = 185. \tag{13}$$

Figure 4 allows one to calculate the time scale τ_r upon which a beam of given velocity $\hat{V}_b$ would be pulled back by the spacecraft. This occurs when $\psi_{sp} = \hat{V}_b^2/2$. For $\hat{V}_b = 1$, this happens at $\tau_r = 154$, 335, and 484 for

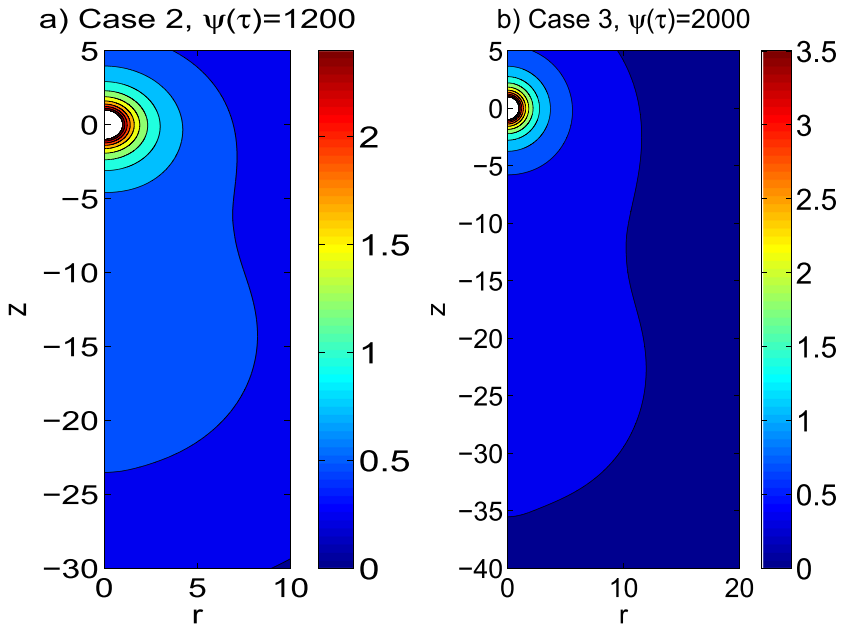

Figure 8. Potential near the spacecraft for Cases 2 and 3, at the time when the amount of electron charge emitted by the beam equals that present in each contactor species at $\tau = 0$. The contactor injection is turned off in these simulations. The background plasma density is $\hat{n}^{bg} = 10^{-4}$ and $\hat{I}_b = 0.093$.

Cases 1, 2, and 3, respectively. For $\hat{V}_b = 2$ one has $\tau_r = 606$, 1000, and 1320, while for $\hat{V}_b = 4$ one has $\tau_r = 1521$, 2321, and 3068.

The fact that the asymptotic evolution of ψ_{sp} in Figure 4 (which is still in the limit $\hat{n}_e^{bg}\tau \ll 1$) is dictated by the spacecraft capacitance (equation (12)) is an indication that the spacecraft is losing contact with the ion contactor cloud. In order to verify this, we look at the plasma densities in Figures 5 and 6 for Case 1. Figure 5 shows the electron density contours corresponding to $\hat{n}_e = 10^2$, 10^1, 10^0, 10^{-1}, and 10^{-2} at various times of the simulation. Note that the background is at $\hat{n}^{bg} \simeq 10^{-4}$ and therefore is not visible in these plots. At time $\tau = 10$ (Figure 5a) the density resembles that of the initial contactor configuration and one can see the $\hat{n}_e = 10^2$ contour and a rather diffused cloud corresponding to $\hat{n}_e = 10^{-2}$. As time progresses and the spacecraft potential rises, electrons from the contactor cloud are pulled back to the spacecraft and the electron density decreases. (In part this is also due to the fact that part of the contactor cloud keeps expanding because of its initial inertia.) For instance, at $\tau = 200$ (Figure 5c) $\hat{n}_e < 10$ and at $\tau = 600$ (Figure 5e) $\hat{n}_e < 1$. At time $\tau = 800$ (Figure 5f) the electron contactor cloud has reduced significantly in size and at time $\tau \simeq 850$ it disappears completely. Figure 6 shows the ion density at the same times and with the same format of Figure 5. In general, the contactor ion clouds keeps expanding because of its inertia and the strong positive charge that is being accumulated on the spacecraft. Consequently, its density decreases. Some density pileup at the back of the ion cloud is also visible. By the time the electron contactor cloud has been completely reabsorbed by the spacecraft, the ion contactor cloud has moved past $z \simeq -6$ and its density is $\hat{n}_i < 1$. Figure 6 shows clearly that the connection between the spacecraft and the ion contactor cloud is lost. Note also that our simulations show no evidence that the expanding ion contactor

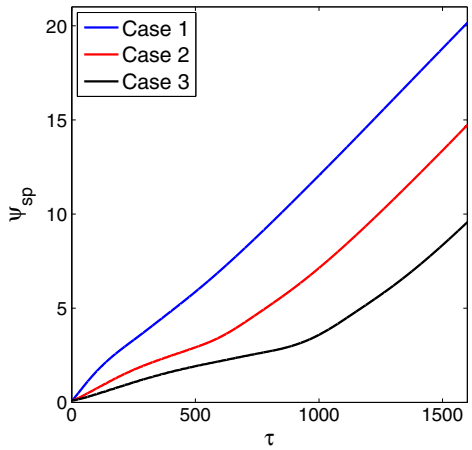

Figure 9. Spacecraft potential versus time starting from the three initial contactor configurations described in section 3, with the injection of the contactor turned on while the beam is emitted but with $\hat{I}_b = 0.374$ ($\hat{I}_i^{cont} = 0.187$). The background plasma density is $\hat{n}^{bg} = 10^{-4}$.

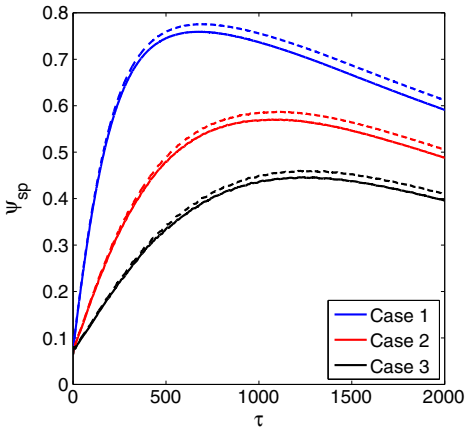

Figure 10. Spacecraft potential versus time starting from the three initial contactor configurations described in section 3, with the injection of the contactor turned on while the beam is emitted. The dashed lines correspond to the cases where the electron beam and the contactor are injected in vacuum (i.e., $\hat{n}^{bg} = 0$). The background plasma density is $\hat{n}^{bg} = 10^{-4}$, $\hat{I}_b = 0.093$, and $\hat{I}_i^{cont} = 0.187$.

cloud is being neutralized by the background plasma. This suggests that even if contact between the spacecraft and the ion contactor cloud was maintained (by having the contactor turned on during beam emission but with $\hat{I}_b > \hat{I}_i^{cont}$), the ion contactor cloud could fail to collect electrons from the background plasma.

Figure 7 shows a zoom of the electrostatic potential at various times for Case 1. Recall that the potential is zero at the outer boundary $\rho_2 = 50$. At the early times, Figure 7a, one can see a shallow virtual anode in front of the contactor injection point. It is interesting to note that the contactor expansion remains roughly quasi-neutral, as can be seen in Figures 7b and 7c. However, as the ion contactor cloud is losing contact with the spacecraft, the potential starts to develop a large, spherically symmetric gradient near the spacecraft. At later times, when the electron contactor cloud has been absorbed and the ion cloud has spread further away from the spacecraft, the effect of the diffused ion contactor cloud becomes less evident and the potential becomes spherically symmetric up to $|z| \sim 5$. Figure 8 shows the potential for Cases 2 and 3 at the times corresponding to when the total electron charge emitted by the beam is approximately equal to the charge present in each contactor species at $\tau = 0$. Compared with Figure 7c for Case 1, one can see that a larger emitted charge (and a larger contactor cloud) induces a larger differential between the spacecraft potential and the potential of the ion cloud. For Case 2, the potential in the plateau region extending between $-22 < z < -10$ and $r < 8$ is $\psi \approx 0.54$ while $\psi_{sp} = 2.64$. For Case 3, the plateau is between $-35 < z < -15$ and $r < 12$ with $\psi \approx 0.38$ versus $\psi_{sp} = 3.86$.

Figure 9 shows the spacecraft potential for simulations with the contactor injection kept on during beam emission but with $\hat{I}_b = 0.374 = 2\hat{I}_i^{cont}$. After an initial transient controlled by the size of the contactor cloud, the curves for Cases 1 and 2 grow linearly in time with a slope given by

$$\frac{d\psi_{sp}}{d\tau} \simeq \frac{\hat{I}_b - \hat{I}_i^{cont}}{\hat{C}_{sp}} = 0.15, \tag{14}$$

in good agreement with its numerical evaluation at the end of the simulation, $d\psi_{sp}^{num}/d\tau \simeq 0.14$. As before, the electron contactor cloud is reabsorbed completely. Interestingly, the spacecraft is able to emit ions (since the spacecraft potential becomes quite large) and maintains contact with the ion contactor cloud. Nevertheless, the late-time evolution in Figure 9 is governed by the spacecraft capacitance and not by the capacitance of the ion cloud. The fact that the potential grows linearly with time indicates that the contactor fails to draw a large neutralizing current from the background.

Figure 10 shows the spacecraft potential for the same conditions of Figure 4 ($\hat{I}_b = 0.093$) but maintaining the contactor injection after the electron beam has been turned on ($\hat{I}_i^{cont}$=0.187). For comparison, Figure 10 also shows the result from the simulations that were carried out in *Delzanno et al.* [2015] for the same parameters but with the beam and the contactor injected in vacuum (i.e., $\hat{n}_{bg} = 0$). In those simulations carried out in *Delzanno et al.* [2015] it was determined that the net ion emission from the outer surface of the contactor plasma cloud was balancing the current of the electron beam. One can see in Figure 10 that the effect of the background plasma is negligible in this case: it supplies a rather small current that reduces the peak of the spacecraft potential slightly relative to the case without background plasma. Unlike the case of Figure 4, one can see that the spacecraft potential initially rises (with the same slope that was calculated for the cases in Figure 4), it peaks and then decreases. Thus, any beam with velocity $\hat{V}_b > \sqrt{2\psi_{sp}^{max}}$ (ψ_{sp}^{max} is the maximum of the spacecraft potential) would be emitted in this scenario, a rather modest requirement considering also that larger initial contactor clouds decrease ψ_{sp}^{max}. In comparison with Figure 4, a beam with $\hat{V}_b = 1$ would return to the spacecraft for Cases 1 and 2 but would be emitted for Case 3. Any beam with $\hat{V}_b > 1.3$ would be

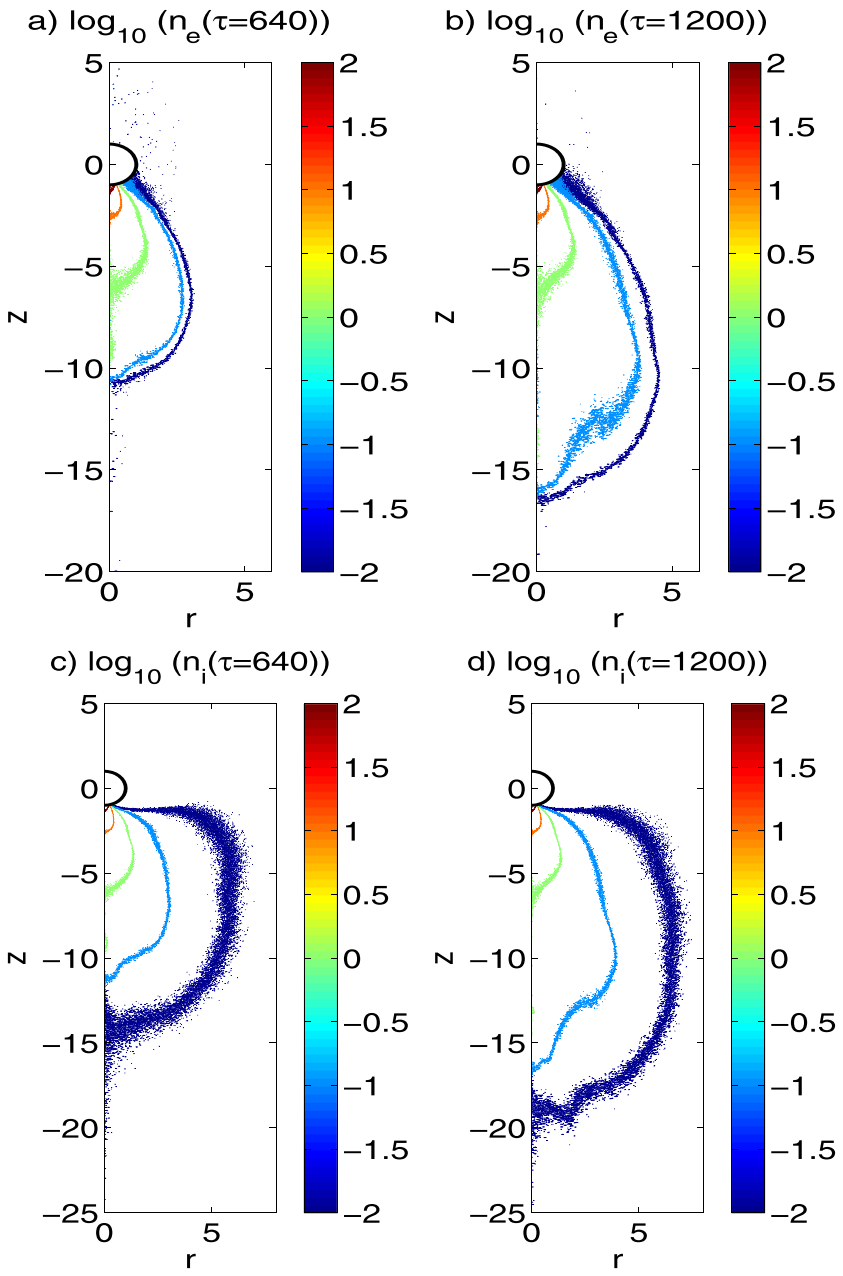

Figure 11. Electron and ion density contours corresponding to $\hat{n} = 10^2, 10^1, 10^0, 10^{-1}$, and 10^{-2} at various times for Case 1. The contactor injection is turned on while the beam is emitted and the background plasma density is $\hat{n}^{bg} = 10^{-4}$, $\hat{I}_b = 0.093$, and $\hat{I}_i^{cont} = 0.187$.

emitted. In these cases where the contactor plasma emission is kept on during the electron beam operation, net ion emission is acting.

Figure 11 shows electron and ion density contours for Case 1 of Figure 10, obtained at two different times. One can see that the continuous injection of the contactor plasma maintains contact between the spacecraft and the contactor cloud. Figure 11 also shows that the contactor cloud has a steady state quasi-neutral component (for densities $\hat{n}_e = \hat{n}_i \gtrsim 1$ in Figure 11, where the ion and electron density contours overlap almost perfectly) and a nonneutral component ($\hat{n}_e \sim \hat{n}_i \lesssim 0.1$) that keeps expanding. As discussed in *Delzanno et al.* [2015], it is the ability to emit ions off the quasi-neutral part of the contactor cloud that allows the spacecraft potential to decrease asymptotically in time (recall that $\hat{I}_b < \hat{I}_i^{cont}$).

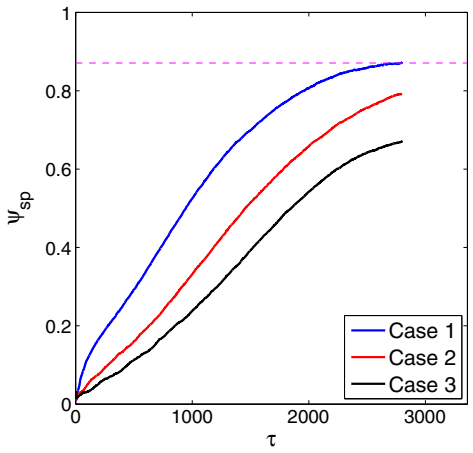

Figure 12. Spacecraft potential versus time starting from the three initial contactor configurations described in section 3, with the injection of the contactor turned off while the beam is emitted. The background plasma density is $\hat{n}^{bg} = 10^{-2}$ and $\hat{I}_b = 0.093$. The dashed line represents the equilibrium value $\psi_{sp}^{eq} \simeq 0.87$ obtained from equation (1).

We have also analyzed the case where the background density is much higher, $\hat{n}^{bg} = 10^{-2}$, again for $\hat{I}_b$=0.093. The spacecraft potential for simulations of Cases 1, 2, and 3 and with the contactor injection turned off when the beam is emitted are presented in Figure 12 (compare with Figure 4 at $\hat{n}^{bg}$=10^{-4}). For these parameters, equation (13) gives a substantially lower equilibrium spacecraft potential $\psi_{sp}^{eq} \simeq 0.86$. Including also the ion collection current in the current balance of equation (1) gives $\psi_{sp}^{eq} \simeq 0.87$. From Figure 12 it can be seen that the spacecraft potential approaches $\psi_{sp}^{eq} \simeq 0.87$ asymptotically, at least for Case 1. Owing to the larger background density, any beam with $\hat{V}_b > 1.3$ would be emitted. Figure 13 shows the spacecraft potential for Cases 1, 2, and 3 when the contactor injection is maintained during the simulations. Compared to Figure 10, one can see that the presence of the background plasma reduces the transient of the spacecraft potential substantially and facilitates beam emission: any beam with $\hat{V}_b > 0.6$ would now be emitted.

5. Conclusions

In this paper, we have performed PIC simulations to investigate the conditions under which a high-voltage electron beam can be stably emitted by a spacecraft in the low-density magnetosphere. We have compared two scenarios, both relying on a high-density contactor plasma emitted by the spacecraft prior to and during beam emission. In the first scenario, dubbed the electron collection route, the contactor plasma has lower current than the electron beam. It is used with the objective of creating a (kilometer-sized) contactor cloud that can collect magnetospheric electrons over a much larger area than that given by the spacecraft. In the second scenario, the contactor plasma has higher current than the beam current. The ions can be emitted off the large, quasi-spherical area of the contactor cloud without encountering the space charge limits typical of ion beam emission in planar geometry and maintain the spacecraft charging under control. For this reason, this scenario has been referred to as the ion emission route. Our simulation results show that the electron collection route is not viable. In the limit when the contactor is fired only prior to the beam, while the spacecraft charges positively driven by beam emission and reabsorbs the contactor electrons, it pushes away the contactor ions. Thus, the spacecraft loses contact with the ion contactor cloud and with it loses the possibility of drawing a large neutralizing current from the background through the large contactor area. In essence, it returns to a situation where the contactor is absent. In the case where the contactor is kept on during beam emission (but with the contactor current lower than the beam current), contact between the spacecraft and the ion contactor cloud can be maintained but the latter fails to draw a large neutralizing current from the background. In a low-density magnetosphere, both cases imply that the spacecraft charges to a very high potential that prevents beam emission. The ion emission route (with the contactor current larger than the beam current), on the other hand, relies only on the contactor cloud reaching an area where ion emission is not space charge limited, independent of the background

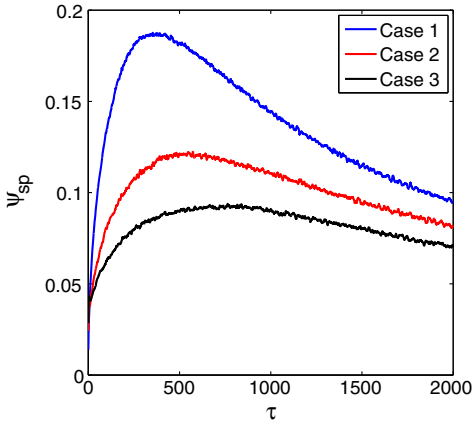

Figure 13. Spacecraft potential versus time starting from the three initial contactor configurations described in section 3, with the injection of the contactor turned on while the beam is emitted. The background plasma density is $\hat{n}^{bg} = 10^{-2}$, $\hat{I}_b = 0.093$, and $\hat{I}_i^{cont} = 0.187$.

density. The presence of the background plasma, however, reduces the transient of the spacecraft potential relative to the case where the contactor is emitted in vacuum and therefore favors beam emission.

In conclusion, the ion emission route offers a pathway to perform beam experiments in the low-density magnetosphere.

Acknowledgments
The data used for this paper were obtained from numerical calculations and are available from the corresponding author upon request.
The authors wish to thank Patrick Colestock and Eric Dors for useful discussions. This work was funded by the Laboratory Directed Research and Development program (LDRD), under the auspices of the National Nuclear Security Administration of the U.S. Department of Energy by Los Alamos National Laboratory, operated by Los Alamos National Security LLC under contract DE-AC52-06NA25396. This research used resources provided by the Los Alamos National Laboratory Institutional Computing Program. J.E.B. was funded by the NASA magnetospheric GI program, the NASA Geospace SRT program, and by the NASA LWS TRT program.

Larry Kepko thanks J.G. Laframboise and another reviewer for their assistance in evaluating this paper.

References

Allen, J., B. Annaratone, and U. de Angelis (2000), On the orbital motion limited theory for a small body at floating potential in a Maxwellian plasma, *J. Plasma Phys.*, *63*, 299–309.
Al'pert, Ya. L., A. V. Gurevich, and L. P. Pitaevskii (1965), *Space Physics with Artificial Satellites*, Plenum Press, New York.
Birdsall, C., and A. Langdon (1985), *Plasma Physics via Computer Simulation*, McGraw-Hill, New York.
Borovsky, J. E., D. J. McComas, M. F. Thomsen, J. L. Burch, J. Cravens, C. J. Pollock, T. E. Moore, and S. B. Mende (2000), Magnetosphere-Ionosphere Observatory (MIO): A multisatellite mission designed to solve the problem of what generates auroral arcs, *Eos Trans. AGU*, *79*(45), F744.
Child, C. D. (1911), Discharge from Hot CaO, *Phys. Rev.*, *32*, 492–511.
Comfort, R. H., T. E. Moore, P. D. Craven, C. J. Pollock, F. S. Mozer, and W. S. Williamson (1998), Spacecraft potential control by the Plasma Source Instrument on the POLAR satellite, *J. Spacecraft Rockets*, *35*, 845–849.
Delzanno, G. L., and X. Z. Tang (2014), Charging and heat collection by a positively charged dust grain in a plasma, *Phys. Rev. Lett.*, *113*, 035002.
Delzanno, G. L., G. Lapenta, and M. Rosenberg (2004), Attractive potential around a thermionically emitting microparticle, *Phys. Rev. Lett*, *92*, 035002.
Delzanno, G. L., E. Camporeale, J. D. Moulton, J. E. Borovsky, E. A. MacDonald, and M. F. Thomsen (2013), CPIC: A curvilinear particle-in-cell code for plasma-material interaction studies, *IEEE Trans. Plasma Sci.*, *41*(12), 3577–3587.
Delzanno, G. L., J. E. Borovsky, M. F. Thomsen, J. D. Moulton, and E. A. MacDonald (2015), Future beam experiments in the magnetosphere with plasma contactors: How do we get the charge off the spacecraft?, *J. Geophys. Res. Space Physics*, doi:10.1002/2014JA020608.
Hallinan, T. J., H. C. Stenbaek-Nielsen, and J. R. Winckler (1978), The Echo 4 electron beam experiment: Television observation of artificial auroral streaks indicating strong beam interaction in the high-latitude magnetosphere, *J. Geophys. Res.*, *83*(A7), 3263–3272, doi:10.1029/JA083iA07p03263.
Hastings, D., and H. Garrett (2004), *Spacecraft-Environment Interactions*, Cambridge Univ. Press, Cambridge.
Hendrickson, R. A., R. W. McEntire, and J. R. Winckler (1975), Echo 1: An experimental analysis of local effects and conjugate return echoes from an electron beam injected into the magnetosphere by a sounding rocket, *Planet. Space Sci.*, *23*, 1431–1444.
Katz, I., J. N. Barfield, J. L. Burch, J. A. Marshall, W. C. Gibson, T. Neubert, W. T. Roberts, W. W. L. Taylor, and J. R. Beattie (1994), Interactions between the space experiments with particle accelerators, plasma contactor, and the ionosphere, *J. Spacecraft Rockets*, *31*, 1079–1084.
Laframboise, J. G. (1966), Theory of spherical and cylindrical Langmuir probes in a collisionless, Maxwellian plasma at rest, *Tech. Rep.*, Univ. of Toronto (Institute for Aerospace Studies), Toronto.
Laframboise, J. G., and L. W. Parker (1973), Probe design for orbit limited current collection, *Phys. Fluids*, *16*(5), 629–636.
Laframboise, J. G., and L. J. Sonmor (1993), Current collection by probes and electrodes in space magnetoplasmas: A review, *J. Geophys. Res.*, *98*(A1), 337–357.
Lavergnat, J. (1982), The French-Soviet experiment ARAKS: Main results, in *Artificial Particle Beams in Space Plasma Studies*, edited by B. Grandal, pp. 87, Plenum, New York.
MacDonald, E. A., J. E. Borovsky, B. Larsen, and E. Dors (2012), A science mission concept to actively probe magnetosphere-ionosphere coupling, *Decadal Survey in Solar and Space Physics papers*.
Mott-Smith, H., and I. Langmuir (1926), The theory of collectors in gaseous discharges, *Phys. Rev.*, *28*, 727.
National Research Council (2012), *Solar and Space Physics: A Science for a Technological Society*, National Academies Press, Washington, D. C.
Nemzek, R. J., and J. R. Winckler (1991), Electron beam sounding rocket experiments for probing the distant magnetosphere, *Phys. Rev. Lett.*, *67*, 987–990.
Nemzek, R. J., P. R. Malcolm, and J. R. Winckler (1992), Comparison of Echo 7 field line length measurements to magnetospheric model predictions, *J. Geophys. Res*, *97*, 1279–1287.
Olsen, R. C. (1985), Experiments in charge control at geosynchronous orbit—ATS-5 and ATS-6, *J. Spacecraft Rockets*, *22*, 254–264.
Parker, L. W., and B. L. Murphy (1967), Potential buildup on an electron emitting ionospheric satellite, *J. Geophys. Res.*, *72*(5), 1631–1636, doi:10.1029/JZ072i005p01631.
Pellat, R., and R. Z. Sagdeev (1980), Concluding remarks on the ARAKS experiments, *Ann. Geophys.*, *36*, 443–446.
Prech, L., Z. Nemecek, J. Safrankova, J. Simunek, V. Truhlik, and N. M. Shutte (1995), Response of the electron energy distribution to an artificially emitted electron beam: APEX experiment, *Adv. Space Res.*, *15*(12), 33–36.
Prech, L., Z. Nemecek, J. Safrankova, and A. Omar (2002), Actively produced high-energy electron bursts within the magnetosphere: The APEX project, *Ann. Geophys.*, *20*, 1529–1538.
Schmidt, R., et al. (1995), Results from active spacecraft potential control on the Geotail spacecraft, *J. Geophys. Res.*, *100*, 17,253–17,260.
Swanson, R. L., J. E. Steffen, and J. R. Winckler (1986), The effect of strong pitch angle scattering on the use of artificial auroral streaks for echo detection—ECHO 5, *Planet. Space Sci.*, *34*, 411–427.
Tang, X.-Z., and G. L. Delzanno (2014), Orbital-motion-limited theory of dust charging and plasma response, *Phys. Plasmas*, *21*, 123708.
Torkar, K., et. al. (2001), Active spacecraft potential for Cluster—Implementation and first results, *Ann. Geophys.*, *19*, 1289–1302.
Wang, J., and S. T. Lai (1997), Virtual anode in ion beam emissions in space: Numerical simulations, *J. Spacecraft Rockets*, *34*(6), 829–836.
Whipple, E. C. (1981), Potentials of surfaces in space, *Rep. Prog. Phys.*, *44*, 1197–1250.
Winckler, J. R. (1980), The application of artificial electron beams to magnetospheric research, *Rev. Geophys. Space Phys.*, *18*, 659–682.
Zhulin, I. A., A. V. Kustov, M. V. Uspensky, and T. V. Miroshnikova (1980), Radar observations of the overdense ionospheric ionization created by the artificial electron beam in the "Zarnitza-2" experiment, *Ann. Geophys.*, *36*, 313–318.